Microtubule detyrosination guides chromosomes during mitosis

Marin Barisic,1,2 Ricardo Silva e Sousa,3* Suvranta K. Tripathy,3* Maria M. Magiera,4,5,6* Anatoly V. Zaytsev,3,7,8 Ana L. Pereira,1,2 Carsten Janke,4,5,6 Ekaterina L. Grishchuk,3†‡ Helder Maiato1,2,9†‡

1Chromosome Instability and Dynamics Laboratory, Instituto de Biologia Molecular e Celular, Universidade do Porto, Rua do Campo Alegre 823, 4150-180 Porto, Portugal. 2Instituto de Investigação e Inovação em Saúde–i3S, Universidade do Porto, Portugal. 3Department of Physiology, Perelman School of Medicine, University of Pennsylvania, Philadelphia, Pennsylvania, USA. 4Institut Curie, 91405 Orsay, France. 5Paris Sciences et Lettres (PSL) Research University, 75005 Paris, France. 6Centre National de la Recherche Scientifique UMR 3348, 91405 Orsay, France. 7Center for Theoretical Problems of Physicochemical Pharmacology, Russian Academy of Sciences (RAS), Moscow, Russia. 8Federal Research and Clinical Centre of Pediatric Hematology, Oncology and Immunology, Moscow, Russia. 9Cell Division Unit, Department of Experimental Biology, Faculdade de Medicina, Universidade do Porto, Alameda Professor Hernâni Monteiro, 4200-319 Porto, Portugal.

*These authors contributed equally to this work. †Corresponding author. E-mail: maiato@ibmc.up.pt (H.M.); gekate@mail.med.upenn.edu (E.L.G.) ‡These authors contributed equally to this work.

Originally published in Science 348(6236), 799–803, May 15, 2015.

DOI: 10.1126/science.aaa5175

Before chromosomes segregate into daughter cells, they align at the mitotic spindle equator, a process known as chromosome congression. Centromere-associated protein E (CENP-E)/Kinesin-7 is a microtubule plus-end–directed kinetochore motor required for congression of pole-proximal chromosomes. Because the plus-ends of many astral microtubules in the spindle point to the cell cortex, it remains unknown how CENP-E guides pole-proximal chromosomes specifically toward the equator. We found that congression of pole-proximal chromosomes depended on specific posttranslational detyrosination of spindle microtubules that point to the equator. In vitro reconstitution experiments demonstrated that CENP-E–dependent transport was strongly enhanced on detyrosinated microtubules. Blocking tubulin tyrosination in cells caused ubiquitous detyrosination of spindle microtubules, and CENP-E transported chromosomes away from spindle poles in random directions. Thus, CENP-E–driven chromosome congression is guided by microtubule detyrosination.

Chromosome congression is the process that leads to the formation of a metaphase plate at the equator of mitotic cells. During congression, peripheral chromosomes are first brought to the vicinity of spindle poles by the microtubule minus-end-directed kinetochore motor Dynein and

INSTITUTO DE INVESTIGAÇÃO E INOVAÇÃO EM SAÚDE
UNIVERSIDADE DO PORTO

Rua Alfredo Allen, 208
4200-135 Porto
Portugal
+351 220 408 800
info@i3s.up.pt
www.i3s.up.pt

are subsequently transported toward the equator by the plus-end–directed kinetochore motor centromere-associated protein E (CENP-E)/Kinesin-7 (1–3). Because different kinetochore motors are able to move chromosomes in opposite directions along anisotropic spindle microtubules, how chromosomes are guided toward the equator remains a critical longstanding question. This might involve spatial cues provided by intracellular gradients, such as the Ran guanosine triphosphate (GTP) gradient, which becomes established around aligned chromosomes (4). We tested this possibility by expressing the dominant negative mutant RanT24N (5), which fails to bind GTP and inhibits RCC1-dependent RanGTP gradient formation from chromosomes, but found no major congression problems in human U2OS cells (fig. S1). Alternatively, the activity and/or affinity of kinetochore motors to microtubules might itself be regulated (for example, by phosphorylation) (6, 7). This model would account for the relative dominance of different kinetochore motors in time and space, but it fails to explain the biased motion of pole-proximal chromosomes toward the equator. A third hypothesis predicts that kinetochore motors are sensitive to spatial cues encoded by the microtubule tracks they move on, which determine the direction of chromosome motion. These spatial cues may result from different stability within spindle microtubules (for example, astral versus kinetochore microtubules), or from their different organization (for example, individual versus bundled microtubules). However, recent work has shown that stable kinetochore microtubule bundles are dispensable for CENP-E–mediated chromosome congression (8), suggesting a different mechanism.

One possibility is that tubulin posttranslational modifications (PTMs) generate specific cues that guide CENP-E along specific spindle microtubules. This so-called “tubulin code” has been proposed to contribute to subcellular differentiation of microtubules (9, 10), and tubulin acetylation and detyrosination are specifically enriched on stable spindle microtubules that point to the equator (11–13). Tubulin acetylation and detyrosination regulate Kinesin-1-dependent transport in neurons (14–16), and recent in vitro reconstitution experiments have also demonstrated subtle but direct effects of tubulin PTMs on the motor activities of Kinesin-2, Kinesin-13, and Dynein (17).

To test whether tubulin detyrosination and acetylation are required for chromosome congression, we perturbed the function of enzymes responsible for specific catalytic steps (fig. S2, A and B). To modulate tubulin detyrosination in human U2OS cells, we overexpressed tubulin tyrosine ligase (TTL), which specifically converts soluble a-tubulin to its tyrosinated form (18). In parallel, we inhibited tubulin carboxypeptidase (TCP) with the cell-permeable drug parthenolide (19), thus preventing removal of the C-terminal tyrosine from polymerized α-tubulin (10). Both treatments specifically decreased tubulin detyrosination without affecting polyglutamylation (Fig. 1A and fig. S3) and reduced the detyrosination of spindle microtubules pointing to the equator (Fig. 1B and fig. S4A). These cells consistently showed misaligned pole-proximal chromosomes and delayed mitotic progression, phenocopying CENP-E inhibition (Fig. 1B, fig. S4B, movie S1). In contrast, perturbation of tubulin acetylation had no effect on chromosome congression (fig. S5, A to C). Thus, detyrosination of spindle microtubules pointing to the equator is required for congression of poleproximal chromosomes.

Whereas CENP-E is mostly associated with kinetochores during early mitosis, we noticed that CENP-E-green fluorescent protein (GFP) expressed under control of its own promoter (20) specifically colocalized with the few detyrosinated microtubules (D-MTs) present in HeLa cells in G2 (fig. S6, A and B) (21). Moreover, inhibition of tubulin detyrosination with parthenolide led to CENP-E dissociation from these microtubules (figs. S4A and S7, A and B, and movie S2), suggesting that tubulin detyrosination promotes the interaction between CENP-E and microtubules in vivo. To test whether this tubulin PTM affects CENP-E directly, we reconstituted CENP-E motility in vitro using purified components. Brain tubulin was not suitable for these

INSTITUTO
DE INVESTIGAÇÃO
E INOVAÇÃO
EM SAÚDE
UNIVERSIDADE
DO PORTO

Rua Alfredo Allen, 208
4200-135 Porto
Portugal
+351 220 408 800
info@i3s.up.pt
www.i3s.up.pt

experiments because it is highly detyrosinated and carries many other PTMs (Fig. 2A). We thus developed a method to purify tyrosinated tubulin from HeLa cells by using cycles of polymerization and depolymerization (22). A fraction of this tubulin was then treated with carboxypeptidase A to produce detyrosinated tubulin (Fig. 2A). These purified proteins were used to polymerize T- and D-MTs, and motility of recombinant CENP-E-GFP was examined by using total internal reflection fluorescence microscopy (fig. S8A and movie S3). CENP-E bound to and moved processively and unidirectionally on both types of microtubules, but it was slower on T-MTs as compared with D-MTs: 26.7 ± 0.4 versus 31.3 ± 0.7 mm/min, respectively (Fig. 2B and fig. S8B). Moreover, there was a ~60% decrease in the characteristic length of CENP-E runs on T-MTs compared with D-MTs (0.97 ± 0.07 versus 1.55 ± 0.06 mm), implying that CENP-E walks more processively on D-MTs assembled in vitro.

We next investigated the force produced by single CENP-E motors using a stationary optical trap (23). CENP-E motors carrying a C-terminal 6xHis-tag were linked to 0.54-µm streptavidin-coated polystyrene beads with biotinylated antibodies to 6X His tag. The beads were then positioned near the microtubule by using an infrared laser, and their motility was examined in a buffer with physiological levels of adenosine triphosphate. Bead-microtubule binding frequencies were similar for these two types of microtubules (0.45 and 0.41 s^{-1} for T- and D-MTs, respectively). As the bead moved away from the center of the trap because of CENP-E motor activity, it experienced greater trapping force and eventually detached and snapped back to the center of the trap (movie S4). These repeated motions led to the characteristic displacement spikes recorded with a quadrant photodetector (Fig. 2C). Whereas large forces generated by CENP-E were infrequent on T-MTs, the force values on D-MTs extended into the 8 pN range (Fig. 2C and fig. S9C). Consistently, the average duration of the force spikes was shorter on T-MTs as compared with D-MTs (0.49 ± 0.02 versus 0.79 ± 0.05 s) (fig. S9D). Thus, CENP-E is unable to sustain large loads onT-MTs, which is in line with the persistence of poleproximal chromosomes after inhibition of microtubule detyrosination in spindles (Fig. 1B).

To investigate the CENP-E stepping mechanism on different microtubule lattices, we analyzed high-resolution bead recordings (Fig. 2, D and E). On both types of microtubules, the average step size was ~8 nm (fig. S9E), which is as expected based on tubulin dimer spacing in the microtubule lattice (24). Backward steps were frequently observed, and with increasing trap load, the probability of a forward step decreased more gradually for CENP-E (Fig. 2F and fig. S9F) than for Kinesin-1 (25, 26). Although the forward stepping of CENP-E was slightly less frequent on T-MTs compared with D-MTs, the overall dependency of CENP-E stepping on the resisting force was similar on these two lattices. The average dwell time between the steps for the entire force range was also similar on T- and D-MTs (fig. S9G). We further observed a slightly shorter dwell time at low force on D-MTs, which is consistent with the faster velocity of CENP-E walking on this type of microtubules (Fig. 2G). CENP-E responded to larger loads by lengthening its dwells on D-MTs, but not on T-MTs. Under the load, CENP-E also detached less frequently from D-MTs (Fig. 2H). As a result, the peak force for CENP-E detachment was shifted to significantly higher values on D-MTs (Fig. 2I), indicating that the effect of tubulin detyrosination is exerted mostly on CENP-E detachment, rather than stepping. Thus, CENP-E can carry a significantly larger load on D-MTs in vitro.

Our data support a model in which CENPE–dependent transport of pole-proximal chromosomes toward the spindle equator requires microtubule tracks that are detyrosinated. Therefore, increasing tubulin detyrosination should disrupt the biased motion of pole-proximal chromosomes toward the equator and cause their delivery to inappropriate cellular locations. To test this, we increased tubulin detyrosination by depleting TTL by means of RNA interference (RNAi) in U2OS cells (fig. S10A). TTL depletion caused ubiquitous detyrosination of spindle microtubules (including astral microtubules) during early mitosis (fig. S10B) (27). Of TTL-

INSTITUTO
DE INVESTIGAÇÃO
E INOVAÇÃO
EM SAÚDE
UNIVERSIDADE
DO PORTO

Rua Alfredo Allen, 208
4200-135 Porto
Portugal
+351 220 408 800
info@i3s.up.pt
www.i3s.up.pt

depleted cells, 65% delayed mitotic progression and failed to congress all the chromosomes (Fig. 3A and movie S5). In these cells, the pole-proximal chromosomes did not remain stuck at the spindle poles, as observed after CENP-E inhibition or after blocking tubulin detyrosination, but were transported in various directions, including toward the cell cortex (Fig. 3, A and B). This suggests that the spatial cues that normally guide CENP-E toward the equator were disrupted. CENP-E inhibition in live TTL-depleted cells significantly decreased the transport of chromosomes away from spindle poles (Fig. 3, A and B). This was confirmed in a large population of fixed cells by use of a quantitative monopolar spindle configuration assay (Fig. 4, A to C) (1), indicating that the random transport of chromosomes along ubiquitously detyrosinated spindle microtubules after TTL RNAi is mediated by CENP-E.

Taken together, our work establishes the specific molecular mechanism that guides CENP-E-dependent chromosome motion toward the cell equator. This mechanism is based on the ability of CENP-E to transport pole-proximal chromosomes preferentially on detyrosinated microtubule tracks, which are normally oriented toward the spindle equator (fig. S11). We propose that microtubule detyrosination works as a navigation system that guides kinetochore motors during cell division, ultimately contributing to faithful chromosome segregation.

REFERENCES AND NOTES

1. M. Barisic, P. Aguiar, S. Geley, H. Maiato, Nat. Cell Biol. 16, 1249–1256 (2014).
2. T. M. Kapoor et al., Science 311, 388–391 (2006).
3. C. E. Walczak, S. Cai, A. Khodjakov, Nat. Rev. Mol. Cell Biol. 11, 91–102 (2010).
4. P. Kalab, R. Heald, J. Cell Sci. 121, 1577–1586 (2008).
5. T. Kiyomitsu, I. M. Cheeseman, Nat. Cell Biol. 14, 311–317 (2012).
6. Y. Kim, A. J. Holland, W. Lan, D. W. Cleveland, Cell 142, 444–455 (2010).
7. J. Whyte et al., J. Cell Biol. 183, 819–834 (2008).
8. S. Cai, C. B. O'Connell, A. Khodjakov, C. E. Walczak, Nat. Cell Biol. 11, 832–838 (2009).
9. K. J. Verhey, J. Gaertig, Cell Cycle 6, 2152–2160 (2007).
10. C. Janke, J. Cell Biol. 206, 461–472 (2014).
11. G. G. Gundersen, J. C. Bulinski, J. Cell Biol. 102, 1118–1126 (1986).
12. P. J. Wilson, A. Forer, Cell Motil. Cytoskeleton 14, 237–250 (1989).
13. G. G. Gundersen, M. H. Kalnoski, J. C. Bulinski, Cell 38, 779–789 (1984).
14. N. A. Reed et al., Curr. Biol. 16, 2166–2172 (2006).
15. Y. Konishi, M. Setou, Nat. Neurosci. 12, 559–567 (2009).
16. J. W. Hammond et al., Mol. Biol. Cell 21, 572–583 (2010).
17. M. Sirajuddin, L. M. Rice, R. D. Vale, Nat. Cell Biol. 16, 335–344 (2014).
18. K. Ersfeld et al., J. Cell Biol. 120, 725–732 (1993).
19. X. Fonrose et al., Cancer Res. 67, 3371–3378 (2007).
20. I. Poser et al., Nat. Methods 5, 409–415 (2008).
21. T. J. Yen, G. Li, B. T. Schaar, I. Szilak, D. W. Cleveland, Nature 359, 536–539 (1992).
22. Materials and methods are available as supplementary materials on Science Online.
23. N. Gudimchuk et al., Nat. Cell Biol. 15, 1079–1088 (2013).

24. H. Yardimci, M. van Duffelen, Y. Mao, S. S. Rosenfeld, P. R. Selvin, Proc. Natl. Acad. Sci. U.S.A. 105, 6016–6021 (2008).

25. N. J. Carter, R. A. Cross, Nature 435, 308–312 (2005).

26. M. Nishiyama, H. Higuchi, T. Yanagida, Nat. Cell Biol. 4, 790–797 (2002).

27. L. Peris et al., J. Cell Biol. 174, 839–849 (2006).

ACKNOWLEDGMENTS

We thank F. I. Ataullakhanov for help with the laser trap and data analysis; A. Kiyatkin, V. Mustyatsa, M. Molodtsov, A. Gautreau, G. Lakisic, and M. Barisic for technical assistance; and members of our laboratories for stimulating discussions. This work was supported by National Institutes of Health grant R01-GM098389 and RSG-14-018-01-CCG from the American Cancer Society to E.L.G.; by the Institut Curie, the Centre National de la Recherche Scientifique, the Institut National de la Santé et de la Recherche Médicale, the L'Agence Nationale de la Recherche (ANR) award ANR-12-BSV2-0007, INCA_6517, ANR-10-LBX-0038, part of the IDEX Idex PSL, ANR-10-IDEX-0001-02 PSL to C.J.; and Fundação Luso-Americana para o Desenvolvimento (FLAD) Life Science 2020 and PRECISE grant from the European Research Council to H.M. A.V.Z. is supported by the RAS Presidium Grants "Mechanisms of the Molecular Systems Integration," "Molecular and Cell Biology programs," and Russian Fund for Basic Research Grant 12-04-00111-a and 13-00-40188. R.S.S. is supported by a fellowship from the Programa Graduado em Áreas da Biologia Básica e Aplicada (GABBA) PhD program from the University of Porto. A.L.P. is supported by fellowship SFRH/BPD/66707/2009 from Fundação para a Ciência e a Tecnologia of Portugal. M.B., R.S.S., S.K.T., M.M.M., C.J., E.L.G., and H.M. designed the experiments; M.B. performed all experiments in cells; M.M.M. established and performed the tubulin purification protocol from HeLa cells; R.S.S. performed single-molecule experiments; S.K.T. performed force measurements; A.L.P. provided reagents; all authors analyzed data; H.M., E.L.G., and M.B. wrote the paper, with contributions from all authors; H.M. conceived and coordinated the project. Data described can be found in the main figures and supplementary materials. The authors declare no conflict of interests.

INSTITUTO
DE INVESTIGAÇÃO
E INOVAÇÃO
EM SAÚDE
UNIVERSIDADE
DO PORTO

Rua Alfredo Allen, 208
4200-135 Porto
Portugal
+351 220 408 800
info@i3s.up.pt
www.i3s.up.pt

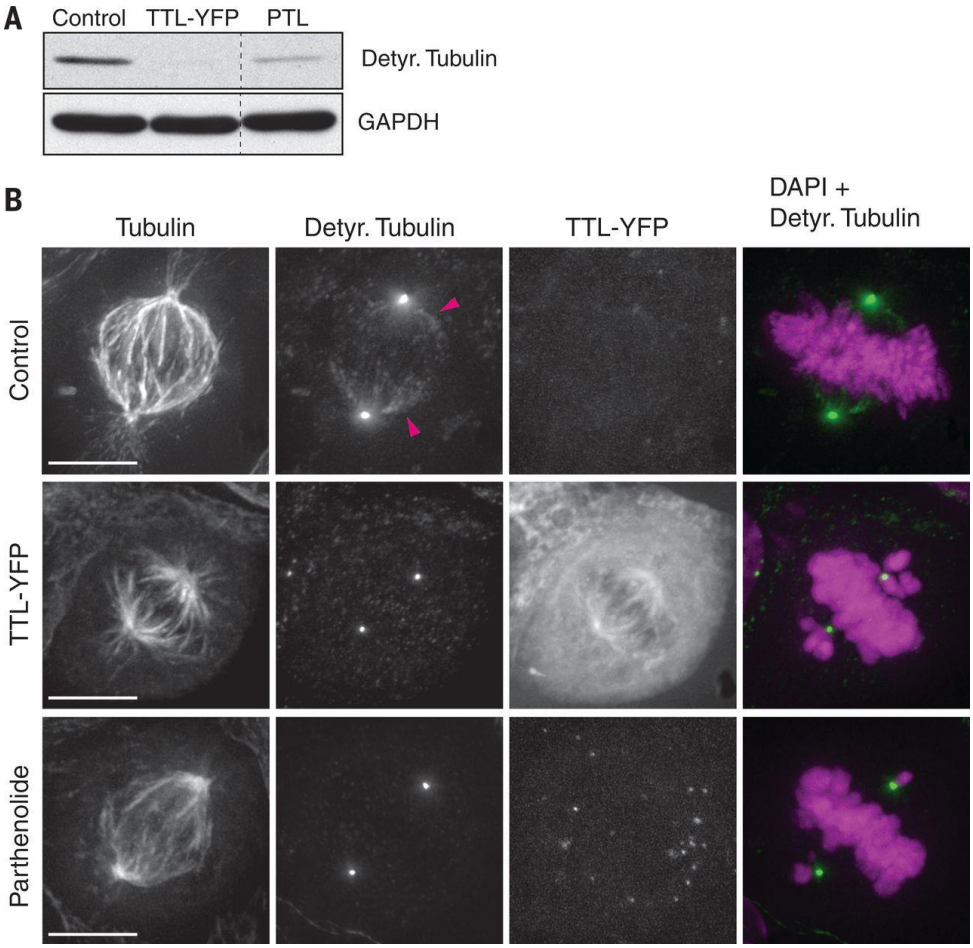

Fig. 1. Chromosome congression requires spatially regulated detyrosination of spindle microtubules. (A) Microtubule detyrosination was examined by means of immunoblotting with detyrosinated tubulin antibodies. Protein lysates of U2OS cells were obtained 24 hours after TTL–yellow fluorescent protein (YFP) transfection and 4 hours after adding parthenolide (20 μM). Glyceraldehyde-3-phosphate dehydrogenase (GAPDH) was used as loading control. (B) Deconvolved immunofluorescence images of U2OS cells stained for DNA [4′,6-diamidino-2-phenylindole (DAPI), magenta], α-tubulin, and detyrosinated tubulin (green). TTL-YFP signal was detected by means of direct fluorescence. Arrowheads highlight detyrosinated spindle microtubules in control cells. Detyrosination of spindle microtubules is undetectable after TTL-YFP overexpression or treatment with parthenolide. Scale bar, 10 μm.

INSTITUTO
DE INVESTIGAÇÃO
E INOVAÇÃO
EM SAÚDE
UNIVERSIDADE
DO PORTO

Rua Alfredo Allen, 208
4200-135 Porto
Portugal
+351 220 408 800
info@i3s.up.pt
www.i3s.up.pt

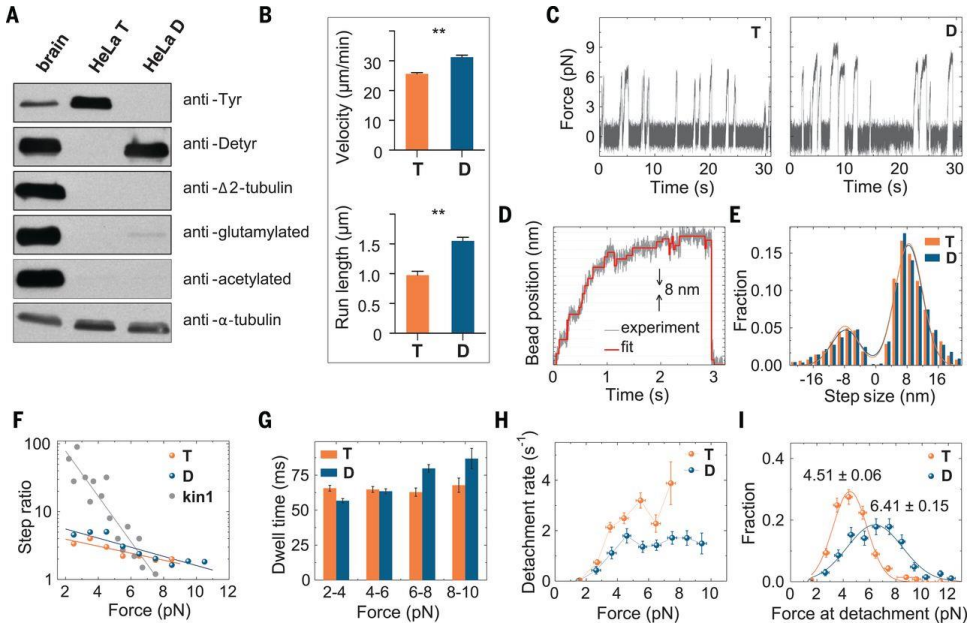

Fig. 2. CENP-E motility is enhanced on detyrosinated microtubules in vitro. (A) Immunoblot of purified tubulin from porcine brain or HeLa cells before (T) and after (D) detyrosination with carboxypeptidase A. Antibodies against tyrosinated, detyrosinated, Δ2, glutamylated (GT335), and acetylated tubulin were used to assess posttranslational modifications. Antibody to α-tubulin demonstrates similar amounts of tubulin in different lanes. (B) Mean velocity and characteristic run length of CENP-E for T-MTs (N = 3 independent experiments, n = 257 molecules) and D-MTs (N = 4 independent experiments, n = 401). Error bars are SEM; **P ≤ 0.01 based on unpaired t test with 95% confidence. (C) Typical traces of bead motions on T- and D-MTs, plotted as force versus time. (D) Example trace of CENP-E bead in a laser trap with step-size fit. (E) Step-size histograms were fit by the sum of two Gaussians (lines). Positive steps were away from the trap's center. Number of forward steps was 5146 and 3427, and number of backward steps was 1731 and 1114, for T- and D-MTs, respectively. (F) Ratio of forward to backward steps for CENP-E in comparison with Kinesin-1 [data from (25, 26)] with theoretical fittings for ratio >1. (G) Characteristic dwell times as a function of force within 2-pN bins. Total number of dwells for all forces was 6877 and 4541 for T- and D-MTs, respectively. (H) CENP-E detachment rate under load. Error bars for detachment rate were calculated by dividing the square root of the number of detachments by the total time within each bin. Error bars for force are SEM for measurements in each bin. (I) Histograms of detachment force with Gaussian fits. Numbers are the mean ± SEM, n = 491 detachments for T-MTs, and 269 for D-MTs. Vertical error bars are square roots of the number of detachments normalized by the total number of detachments.

INSTITUTO
DE INVESTIGAÇÃO
E INOVAÇÃO
EM SAÚDE
UNIVERSIDADE
DO PORTO

Rua Alfredo Allen, 208
4200-135 Porto
Portugal
+351 220 408 800
info@i3s.up.pt
www.i3s.up.pt

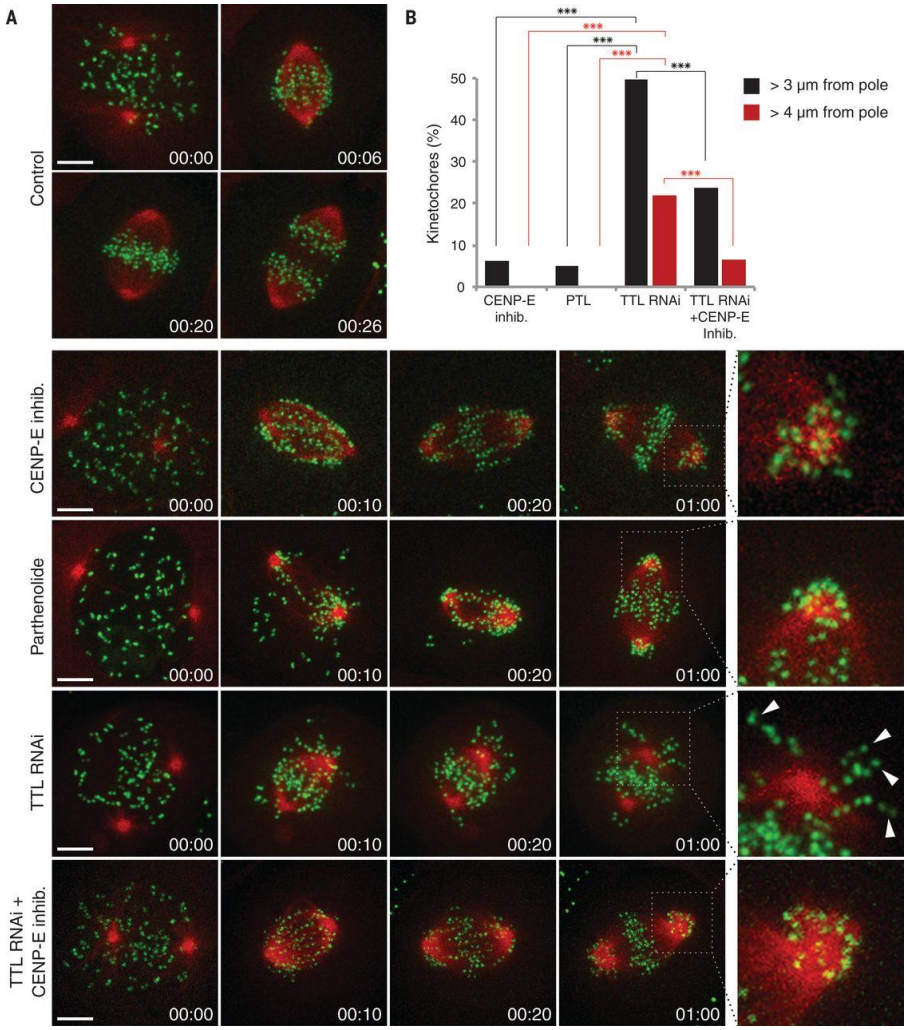

Fig. 3. Chromosomes cannot complete congression in TTL-depleted cells and are randomly transported away from the spindle pole by CENP-E. (A) Spinning-disk confocal imaging of live U2OS cells stably expressing CENP-A–GFP and mCherry-tubulin. Chromosome congression was impaired in 100% of cells treated either with CENP-E inhibitor (13 cells, three independent experiments) or parthenolide (nine cells, two independent experiments). Chromosome congression was impaired in 65% of cells depleted of TTL (23 cells, three independent experiments). Arrowheads highlight kinetochores transported away from the spindle pole toward the cell cortex. Enlarged insets highlight polar regions. Scale bar, 5 mm. Time is hours:min. (B) Quantification of the percentage of pole-proximal chromosomes that were transported away from spindle poles in the different conditions. *N* (CENPE inh.) = 311 kinetochores from 10 cells, three independent experiments; *N* (parthenolide) = 388 kinetochores from 7 cells, two independent experiments; *N* (TTL RNAi) = 311 kinetochores from 18 cells, three independent experiments. *N* (TTL RNAi+CENP-E inh) = 720 kinetochores from 17 cells, three independent experiments. Asterisks indicate z test significance values; ***P < 0.001.

INSTITUTO DE INVESTIGAÇÃO E INOVAÇÃO EM SAÚDE
UNIVERSIDADE DO PORTO

Rua Alfredo Allen, 208
4200-135 Porto
Portugal
+351 220 408 800
info@i3s.up.pt
www.i3s.up.pt

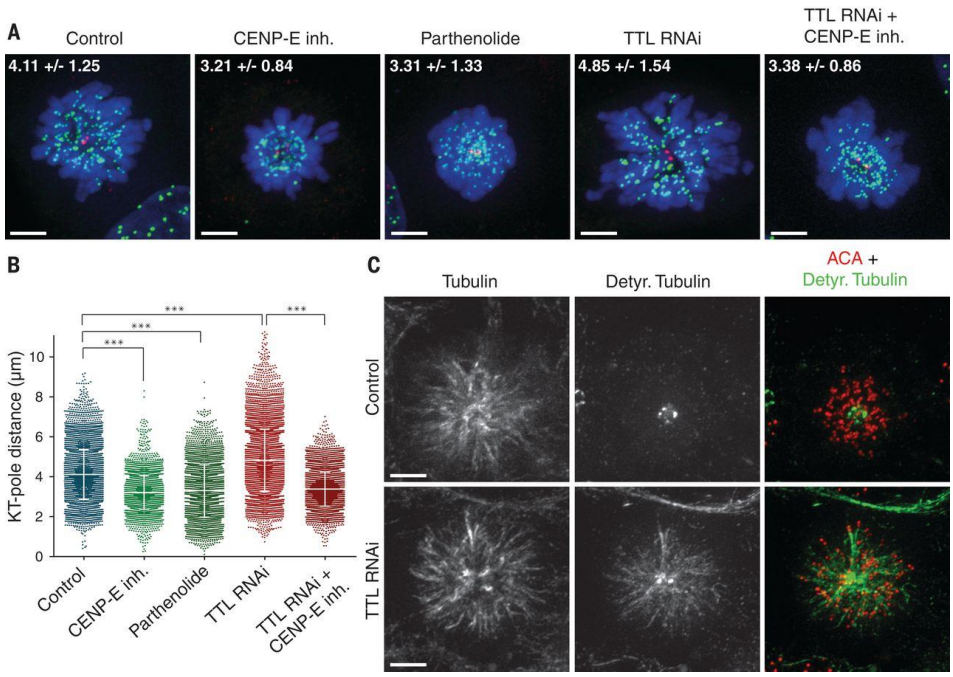

Fig. 4. CENP-E–dependent transport of pole-proximal chromosomes along ubiquitously detyrosinated spindle microtubules after TTL RNAi. (A) U2OS cells treated with the kinesin-5 inhibitor S-Trytil-L-Cysteine (STLC) and immunostained for DNA (DAPI, blue), kinetochores [anti-centromere antibodies (ACA), green] and centrioles (centrin = red). Maximum-intensity projection images of representative examples for each condition are shown. Numbers indicate mean kinetochore-to-pole distances ± SD of the pooled data from at least two independent experiments per condition. Scale bar, 5 mm. (B) Quantification of kinetochore (KT) to pole distances in STLC-treated cells under different conditions; *n* (control) = 7185 kinetochores from 56 cells, three experiments; *n* (CENP-E inh) = 3877 kinetochores from 34 cells, two experiments; *n* (Parthenolide) = 3611 kinetochores from 30 cells, two experiments; *n* (TTL RNAi) = 8239 kinetochores from 61 cells, four experiments; *n* (TTL RNAi + CENP-E inh) = 5458 kinetochores from 45 cells, two experiments. Asterisks indicate Mann-Whitney U test significance values; ***P < 0.001. (C) Deconvolved immunofluorescence images of STLC-treated U2OS cells stained for α-tubulin, detyrosinated tubulin, and ACA. Detyrosination of spindle microtubules was highly increased after TTL RNAi. Scale bar, 5 µm.

INSTITUTO
DE INVESTIGAÇÃO
E INOVAÇÃO
EM SAÚDE
UNIVERSIDADE
DO PORTO

Rua Alfredo Allen, 208
4200-135 Porto
Portugal
+351 220 408 800
info@i3s.up.pt
www.i3s.up.pt